



First application of plutonium in soil erosion research on terraces

Yong-Jing Guan¹ · Wu Chen¹ · Shen-Zhen Wang^{1,2} · Yu-Xin Hua¹ · Qiao-Yan Jing^{1,2} · Zhi-Yong Liu² · Chun-Ping Huang^{1,2} · De-Yu Wang^{1,2} · Hui-Juan Wang¹ · Xian-Wen He³ · Mario De Cesare^{4,5,6} · Liang-Jia Cui¹ · Hua He¹ · Kai-Di Fan¹ · Zi-Chen Guo¹

Received: 17 November 2022 / Revised: 13 February 2023 / Accepted: 18 February 2023 / Published online: 17 April 2023
© The Author(s) 2023

Abstract

The spatial distributions of $^{239+240}\text{Pu}$ and ^{137}Cs in soils from Longji Rice Terraces were investigated to evaluate soil erosion. The activity concentrations of $^{239+240}\text{Pu}$ and ^{137}Cs in the surface soils of the paddy fields were in the range of 0.089–0.734 and 1.80–7.88 mBq/g, respectively. The activities of $^{239+240}\text{Pu}$ and ^{137}Cs showed very similar distribution trends, first increasing and then decreasing with increasing elevation. The $^{240}\text{Pu}/^{239}\text{Pu}$ atom ratios in the surface soils ranged from 0.162 to 0.232. The activities of $^{239+240}\text{Pu}$ and ^{137}Cs in the soil cores tended to be uniformly distributed within the plowed layer and declined exponentially below this depth. The mean soil erosion rates of Longji Rice Terraces estimated by $^{239+240}\text{Pu}$ and ^{137}Cs tracer methods were 5.44 t/(ha·a) and 5.16 t/(ha·a), respectively, which demonstrated that plutonium can replace ^{137}Cs as an ideal tracer for soil erosion research in the future. Landform features are the main factors affecting the distribution of plutonium and ^{137}Cs as well as soil erosion in the Longji Rice Terraces.

Keywords Soil erosion · Plutonium · ^{137}Cs · Tracer method · Terraces

This work was supported by the National Natural Science Foundation of China (No. 12175046), the Guangxi Natural Science Foundation (No. 2021GXNSFBA196001), and the One-Hundred-Talents Program of Guangxi Colleges.

✉ Yong-Jing Guan
yjguan@gxu.edu.cn

- ¹ Guangxi Key Laboratory for Relativistic Astrophysics, School of Physical Science and Technology, Guangxi University, Nanning 530004, China
- ² State Key Laboratory of Radiation Medicine and Protection, School for Radiological and Interdisciplinary Sciences (RAD-X) and Collaborative Innovation Centre of Radiation Medicine of Jiangsu Higher Education Institutions, Soochow University, Suzhou 215123, China
- ³ Radiation-Environment Management and Monitoring Station of Guangxi Zhuang Autonomous Region, Nanning 530222, China
- ⁴ Department of Large Ground Testing Facilities, CIRA - Italian Aerospace Research Centre, 81043 Capua, Italy
- ⁵ Department of Mathematics and Physics, University of Campania “Luigi Vanvitelli”, 81100 Caserta, Italy
- ⁶ INFN - National Institute for Nuclear Physics, Naples Section, 80126 Naples, Italy

1 Introduction

Soil erosion leads to a reduction in soil fertility and degradation of cultivated land, which severely affects agricultural land. Globally, approximately 1.9 billion hm^2 of agricultural land is affected by land degradation and is increasing at a rate of approximately 5–7 million hm^2 per year [1]. Human activities and global warming have resulted in increased soil erosion. Therefore, it is necessary to conduct soil erosion research to provide basic data to prevent land degradation.

Radionuclides have been proven to be powerful tracers for soil erosion investigation [2, 3, 4]. Plutonium and ^{137}Cs ($T_{1/2} = 30.17$ a) are artificial radionuclides mainly produced by artificial nuclear activities [5, 6, 7, 8, 9]. ^{239}Pu ($T_{1/2} = 2.411 \times 10^4$ a) and ^{240}Pu ($T_{1/2} = 6563$ a) were the most important plutonium isotopes. The $^{239+240}\text{Pu}$ released to the environment by atmospheric nuclear tests was approximately 1.26×10^{16} Bq [10]. The atom ratio of $^{240}\text{Pu}/^{239}\text{Pu}$ has become an important factor in investigating the source and migration processes of plutonium in the environment [11]. Accelerator mass spectrometry (AMS) is an effective and robust technique for studying long-lived actinides (e.g., ^{236}U , ^{237}Np , ^{239}Pu , and ^{240}Pu) [12, 13, 14], and inductively coupled plasma mass spectrometry (ICP-MS) is currently

the most widely used technique for measuring actinides because of its lower cost compared to AMS. The distribution, sources, migration, and applications of ^{137}Cs have attracted extensive attention over the past few decades [15, 16, 17, 18, 19, 20]. $^{239+240}\text{Pu}$ and ^{137}Cs in the environment are rapidly and strongly adsorbed by fine soil particles and redistributed within the soil itself [21, 22, 23]. Thus, soil erosion can be traced using the inventories and distribution characteristics of $^{239+240}\text{Pu}$ and ^{137}Cs in the soil [21, 24, 25, 26, 27, 28, 29].

Although ^{137}Cs has been extensively applied to soil erosion in past decades [1, 24, 25, 30, 31, 32], 70% of the total ^{137}Cs deposited by atmospheric nuclear tests in the environment has decayed away so far, which has significantly reduced the sensitivity of ^{137}Cs as a tracer of soil and sediment transport in the future. $^{239+240}\text{Pu}$ is an ideal replacement for ^{137}Cs due to its longer lifetime and the same origin and strong association with soil particles as ^{137}Cs . In recent years, plutonium has been successfully applied to soil erosion studies in the hilly landscape north of Munich, Germany [33, 34]; the Alpine grasslands of Switzerland [27]; the lower Cotter catchment of the Australian Capital Territory [35]; the hillslopes of the Zarivar Lake watershed, Kurdistan Province, Iran [24]; the coastal area of Liaodong Bay in Northeast China [4, 21, 28]; and the hilly gully region of the Loess Plateau in China [36]. However, the study areas are mostly limited to grasslands, woodlands, hillslopes, and commonly sloping cultivated land. To the best of our knowledge, the application of plutonium to soil erosion on terraces of stepped-sloping cultivated lands has not yet been published. Terraces are fields reclaimed on the slopes of mountainous areas where precipitation is abundant. The steepness of the terraces depends on the slope gradient of the original hillside. Excess water from the upper terraces flows to the lower terraces due to gravity. Terraced soil is affected by tilling, loose, and easily washed and carried by rain, particularly during periods of heavy rainfall. Therefore, the steeply sloping rugged mountain topography, loose soil, abundant precipitation, and water flow from the top to bottom create favorable conditions for terrace soil erosion. Soil erosion is directly related to local crop yields and sustainable cultivation owing to the rugged hillside terrain, top-down diffuse water flow, and primitive coupled tillage of the Longji Rice Terraces; therefore, it is necessary to explore a proven means of monitoring local soil erosion. The combination of the long-lived artificial radionuclides $^{239+240}\text{Pu}$ and ^{137}Cs for studying the long-term erosion of terraces would be more convincing. In this study, the activity concentrations of $^{239+240}\text{Pu}$ and ^{137}Cs , and the atomic ratios of $^{240}\text{Pu}/^{239}\text{Pu}$ in soils from the Longji Rice Terraces in Guangxi, China, were measured for the first time. This study analyzed the sources and distribution characteristics of $^{239+240}\text{Pu}$ and ^{137}Cs in the soils of the Longji Rice Terraces,

evaluated the soil erosion status, and verified the feasibility of $^{239+240}\text{Pu}$ instead of ^{137}Cs to study the long-term erosion of the terraces by comparing the erosion rates obtained from the $^{239+240}\text{Pu}$ and ^{137}Cs tracer methods.

2 Material and methods

2.1 Study area

Longji Rice Terraces (109°32'–110°14' E, 25°35'–26°17' N) are located in Longji Town, northwest of Guilin City, Guangxi, China. It is a field developed on Longji Mountain, which belongs to the Yuecheng Mountain range and is the northwest branch of the Nanling Mountain system. The Longji Rice Terraces mainly include Longji Guzhuang Village terraced fields (LGVTF), Ping'an Zhuang terraced fields (PZTF), and Jinkeng Red Yao terraced fields (JRYTF). Longji Rice Terraces are in a subtropical monsoon climate zone affected by the convergence of cold air from the north and warm and humid air from the south, with more frontal rain and fog weather and an annual precipitation was 1800–1900 mm. The elevation of the Longji Rice Terraces is 300–1100 m. Longji Mountain is covered with lush vegetation, so it can store water well. The upper layer of Longji Mountain is permeable sandy loam, which can store water, and the lower layer is impermeable sedimentary rocks, shale bedrock, and slate with good water impermeability, located approximately 1.5–2 m below the surface soil. The excess rainwater that infiltrated the sandy loam flowed out of the cracks in the mountain and down to each terrace. The farming methods of the Longji Rice Terraces are primitive pair plowing and traditional flood irrigation.

2.2 Sample collection

Soil samples were collected from Longji Rice Terrace in November 2021. The sampling locations and information are shown in Fig. 1 and Table 1, respectively. The sample IDs, beginning as “P” and “D,” were taken from PZTF and JRYTF, respectively. The sampling sites on the PZTF (open triangles and pentagons) and JRYTF (solid triangles) are shown in Fig. 1. Triangles and pentagons represent the surface soil and core sites, respectively. Red and yellow lines represent the sampling sites along the slope direction and contour lines, respectively. Fourteen paddy field surface soil samples (0–5 cm, marked by open triangles) and two paddy field soil cores (P1#1 with a depth of 50 cm and P1#2 with a depth of 40 cm, marked by open pentagons) were collected from the PZTF, and 19 paddy field surface soil samples (0–5 cm, marked by solid triangles) were collected from the JRYTF. Surface soil samples were collected along a specified slope direction. Samples from the PZTF and JRYTF

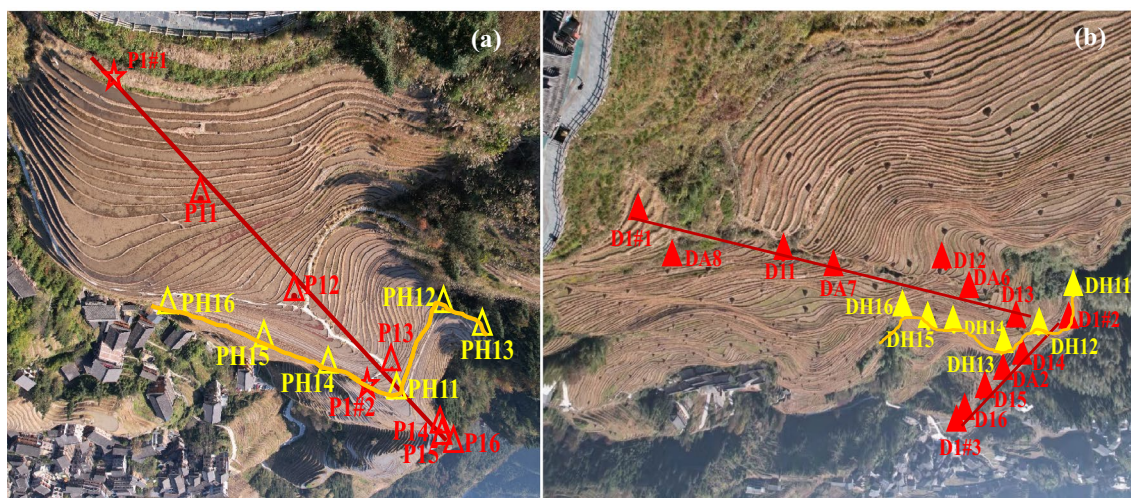


Fig. 1 (Color online) Map showing the soil sampling locations of Longji Rice Terraces in the northwest of Guilin, Guangxi, South China. Triangles and pentagons represent sites of surface soils and cores, respectively. The red lines represent the sampling sites along

the slope direction. **a** PZTF. The yellow line represents the contour line at an elevation of 860 m. **b** JRYTF. The yellow line represents the contour line at an elevation of 970 m.

were collected from high and low elevations along the southwest and southeast slopes, respectively. All soil cores were sliced at 5-cm intervals.

2.3 Sample preparation and measurement

The samples were heated at 100 °C for 12 h until dryness, then crushed, and sieved. After that, the ^{137}Cs activities of the 50 g fine soil samples were measured by an γ spectrometer equipped with a high-purity germanium detector and a lead shielding chamber at a time of 86,400 s. The detailed methodology and spectrometer are described in our previous work [37, 38, 39]. Briefly, A HPGe detector (GEM-C5970; ORTEC, USA) with a counting efficiency of 45% and FWHM of 1.7 keV on 1.33 MeV energy of ^{60}Co was used. ^{137}Cs content was determined by detecting the 661.62 keV signature γ -ray. The detection limit for ^{137}Cs was 0.04 mBq/g. One gram of pretreated soil sample was calcined at 550 °C for 12 h to determine the organic matter content. The organic matter content was calculated as the mass loss before and after the ashing procedure, and was expressed as the percentage loss on ashing for the soil sample.

2.5 g soil sample was weighed for plutonium isotope analysis. Details of the chemical separation and purification processes have been described in previous studies [37, 38, 39]. In brief, 1.82 pg ^{242}Pu was added as a chemical yield tracer to monitor and calculate the chemical recovery of the plutonium isotope analysis, the main analysis processes including digestion, filtration, adjustment of acidity and valence, purification of plutonium with AG1-X8 anion exchange resin, and re-purification of plutonium with AG MP-1 M anion

exchange resin. Finally, the concentrated plutonium solution was placed in a 1.5-mL sample bottle with 4% nitric acid and carried to the College of Radiology and Protection, Soochow University, for measuring $^{239+240}\text{Pu}$ activity and $^{240}\text{Pu}/^{239}\text{Pu}$ atom ratio using sector-field ICP-MS (Finnigan Element 2, Bremen, Germany). The chemical recovery of Pu ranged from 60 to 80%, and the limits of detection for ICP-MS calculated from 3 times the standard deviation of the blank solution (4% HNO_3) were 0.09 fg/mL for ^{239}Pu and 0.14 fg/mL for ^{240}Pu with a counting time of 150 s. The concentration of plutonium isotopes was calculated by subtracting the blank from the measured results of samples, and the measured signal intensities of ^{239}Pu and ^{240}Pu in procedure blank were 8.5 cps and 6.4 cps, respectively.

3 Results and discussion

3.1 Activities of $^{239+240}\text{Pu}$ and ^{137}Cs in soil samples

3.1.1 $^{240}\text{Pu}/^{239}\text{Pu}$ atom ratios, activities of $^{239+240}\text{Pu}$, and ^{137}Cs in surface soil samples

The mean atom ratio of $^{240}\text{Pu}/^{239}\text{Pu}$ in the surface soil samples was 0.195 ± 0.014 ($n=33$), ranging from 0.162 ± 0.013 to 0.232 ± 0.033 (Table 1), which agreed well with the value of the global fallout (0.178 ± 0.023 ($0\text{--}30^\circ\text{N}$)) [40]. This result is consistent with those of previous reports [41, 42, 43, 44, 45, 46]. The result is higher than the $^{240}\text{Pu}/^{239}\text{Pu}$ atom ratio for nuclear weapons-grade plutonium (0.01–0.07, e.g., 0.028–0.037 for the Nagasaki atomic bomb explosion) [47, 48], and lower than those for the Chernobyl nuclear

Table 1 General information of the sampling sites and results of Pu and ^{137}Cs in soil samples

Sample ID	Longitude (E)	Latitude (N)	Elevation (m)	$^{239+240}\text{Pu}$ (mBq/g)	^{137}Cs (mBq/g)	$^{240}\text{Pu}/^{239}\text{Pu}$ atom ratio	OM ^a (%)	Slope (°)
P1#1_0-5	110° 7' 29"	25° 45'39"	930	0.207 ± 0.006	4.04 ± 0.20	0.197 ± 0.015	9.3	–
P11	110° 7' 29"	25° 45'37"	920	0.245 ± 0.009	6.16 ± 0.25	0.189 ± 0.015	9.1	9.4
P12	110° 7' 28"	25° 45'36"	900	0.298 ± 0.010	6.35 ± 0.25	0.203 ± 0.018	9.4	25.1
P13	110° 7' 27"	25° 45'33"	870	0.335 ± 0.011	7.88 ± 0.28	0.194 ± 0.015	11.3	17.5
PH11	110° 7' 27"	25° 45'32"	860	0.330 ± 0.012	6.20 ± 0.25	0.181 ± 0.015	9.9	18.4
P14	110° 7' 26"	25° 45'28"	840	0.259 ± 0.009	5.22 ± 0.23	0.173 ± 0.012	8.9	9.2
P15	110° 7' 26"	25° 45'24"	810	0.228 ± 0.006	4.35 ± 0.21	0.193 ± 0.011	11.1	14.0
P16	110° 7' 26"	25° 45'23"	790	0.089 ± 0.006	1.80 ± 0.13	0.208 ± 0.023	9.9	33.6
PH12	110° 7' 29"	25° 45'32"	860	0.335 ± 0.009	6.31 ± 0.25	0.192 ± 0.013	11.1	–
PH13	110° 7' 29"	25° 45'32"	860	0.249 ± 0.007	5.20 ± 0.23	0.196 ± 0.013	10.3	–
PH14	110° 7' 26"	25° 45'32"	860	0.265 ± 0.009	3.40 ± 0.18	0.187 ± 0.010	10.5	–
PH15	110° 7' 26"	25° 45'32"	860	0.264 ± 0.006	6.27 ± 0.25	0.196 ± 0.010	13.0	–
PH16	110° 7' 27"	25° 45'36"	860	0.232 ± 0.011	4.98 ± 0.22	0.209 ± 0.022	14.4	–
P1#2_0-5	110° 7' 7"	25° 45'32"	860	0.215 ± 0.016	5.13 ± 0.23	0.201 ± 0.018	8.0	–
D1#1_0-5	110° 9' 1"	25° 48'58"	1080	0.224 ± 0.012	4.99 ± 0.22	0.216 ± 0.026	10.0	–
DA8	110° 9' 6"	25° 49'4"	1070	0.089 ± 0.007	2.16 ± 0.14	0.181 ± 0.029	9.0	2.4
D11	110° 9' 2"	25° 48'56"	1050	0.105 ± 0.008	2.23 ± 0.15	0.197 ± 0.027	9.5	4.3
DA7	110° 8' 54"	25° 48'55"	1030	0.158 ± 0.010	3.24 ± 0.17	0.185 ± 0.028	9.0	4.7
D12	110° 9' 3"	25° 48'55"	1020	0.161 ± 0.012	3.79 ± 0.19	0.232 ± 0.033	8.6	2.1
DA6	110° 8' 54"	25° 48'51"	990	0.157 ± 0.010	4.49 ± 0.21	0.188 ± 0.031	8.8	5.8
D13	110° 9' 6"	25° 48'52"	980	0.162 ± 0.014	4.39 ± 0.21	0.204 ± 0.031	8.1	1.6
D1#2_0-5	110° 9' 8"	25° 48'51"	970	0.214 ± 0.017	4.92 ± 0.22	0.176 ± 0.034	9.3	8.5
D14	110° 9' 7"	25° 48'48"	940	0.247 ± 0.015	5.96 ± 0.25	0.201 ± 0.031	9.3	17.5
DA2	110° 9' 6"	25° 48'48"	905	0.243 ± 0.010	6.14 ± 0.25	0.205 ± 0.021	8.7	49.3
D15	110° 9' 7"	25° 48'43"	890	0.318 ± 0.024	6.04 ± 0.25	0.207 ± 0.039	9.3	5.6
D16	110° 9' 9"	25° 48'38"	830	0.190 ± 0.011	4.94 ± 0.22	0.191 ± 0.024	9.2	20.3
D1#3_0-5	110° 9' 9"	25° 48'37"	810	0.109 ± 0.010	3.06 ± 0.17	0.188 ± 0.029	8.8	33.6
DH11	110° 9' 8"	25° 48'52"	970	0.347 ± 0.023	3.44 ± 0.18	0.162 ± 0.013	7.0	–
DH12	110° 9' 7"	25° 48'51"	970	0.380 ± 0.053	4.55 ± 0.21	0.197 ± 0.025	9.8	–
DH13	110° 9' 7"	25° 48'50"	970	0.563 ± 0.057	4.29 ± 0.20	0.228 ± 0.032	9.9	–
DH14	110° 9' 5"	25° 48'51"	970	0.324 ± 0.030	3.86 ± 0.19	0.192 ± 0.021	10.2	–
DH15	110° 9' 4"	25° 48'51"	970	0.464 ± 0.028	3.87 ± 0.19	0.189 ± 0.015	9.0	–
DH16	110° 9' 4"	25° 48'51"	970	0.734 ± 0.046	4.36 ± 0.21	0.203 ± 0.022	9.0	–

^aOrganic matter content

accident (0.403–0.412) [49] and Fukushima nuclear accident (0.303–0.330) [9], indicating there is no regional radioactive contamination in the studied area, so all the Pu and Cs are sourced from the global fallout; then, they can be used as tracers for soil erosion research.

The activities of $^{239+240}\text{Pu}$ and ^{137}Cs in surface soil samples are listed in Table 1. It can be seen that the activities of $^{239+240}\text{Pu}$ range from 0.089 ± 0.007 to 0.734 ± 0.046 mBq/g, with a mean value of 0.264 ± 0.132 mBq/g ($n = 33$), similar to that of surface soils (0.365 ± 0.014 – 0.819 ± 0.066 mBq/g) from Shaodong of Hunan Province in China [43], and within the data range (0.005–1.988 mBq/g) of Chinese surface (≤ 10 cm) soil [50]. $^{239+240}\text{Pu}$ activities in the surface soil of PZTF (0.089 ± 0.006 – 0.335 ± 0.011 mBq/g, with a mean of

0.253 ± 0.064 mBq/g) and JRYTF (0.089 ± 0.007 – 0.734 ± 0.046 mBq/g, with a mean of 0.273 ± 0.168 mBq/g) are similar. The activities of ^{137}Cs in the surface soil samples range from 1.80 ± 0.13 to 7.88 ± 0.28 mBq/g, with a mean value of 4.67 ± 1.38 mBq/g ($n = 33$) which was slightly higher than that of 3.39 mBq/g from Puding County of Guizhou Province [51]. Because all samples were collected from a limited spatial range with a diameter of 1000 m, the large variation in ^{137}Cs activity indicates local alteration after deposition.

As shown in Fig. 2a, the activity of $^{239+240}\text{Pu}$ in the surface soils of the PZTF first increased and then decreased from an elevation of 930–790 m. The maximum value of PZTF appeared at elevations of 860 and 870 m. Figure 2b indicates that $^{239+240}\text{Pu}$ activities in the surface soils of

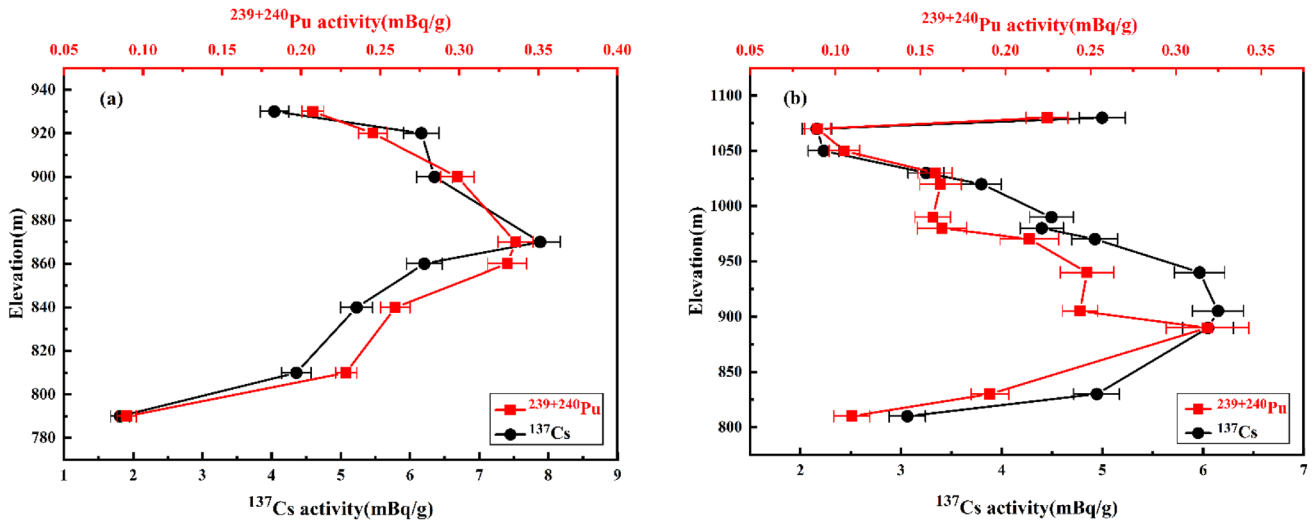


Fig. 2 (Color online) Distributions of $^{239+240}\text{Pu}$ and ^{137}Cs activity in the surface soils of paddy field from Longji Rice Terraces. **a** PZTF. **b** JRYTF

JRYTF, except for the samples at the highest elevation of 1080 m, also showed the same trend as PZTF. The maximum value of the JRYTF appeared at an elevation of 890 m. The same trend in ^{137}Cs activity is observed in Fig. 2. Similarly, the ^{137}Cs inventories of sloping farmland in the southeast of the Qinghai-Tibet Plateau showed a fluctuating increasing and decreasing trend along elevation [25]. All possible factors affecting plutonium and ^{137}Cs concentrations included soil texture, organic matter content, soil moisture, particle size, elevation, and slope gradient. All samples were collected from a small area of rice fields under the same basic environmental conditions, which had the same soil texture, soil moisture, and grain size; therefore, these factors could be excluded. Elevation was also not a major factor affecting the plutonium and ^{137}Cs concentrations in the studied area

because the elevation span of the studied sites was within 300 m, and the concentrations of plutonium and ^{137}Cs did not increase or decrease monotonically with elevation. A strong correlation between $^{39+240}\text{Pu}$ activity concentration and organic matter content was reported in our previous study [39] and by other researchers [52]. However, the surface soil samples of Longji Rice Terraces were all collected from rice paddies with little variation in organic matter content (Table 1), suggesting that landform is more likely to be the main factor in $^{239+240}\text{Pu}$ activity variation relative to organic matter. Landform factors, such as slope gradients, are among the most important factors affecting the spatial variation in soil erosion rates [53, 54]. Figure 3a shows the distributions of $^{239+240}\text{Pu}$ and ^{137}Cs in surface soils at an elevation of 860 m in the PZTF. The activities

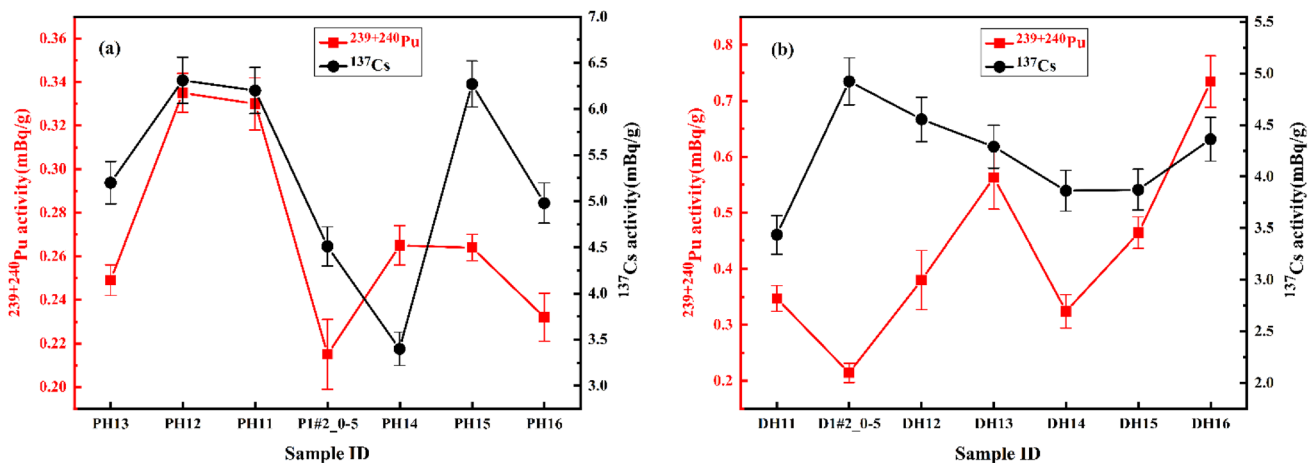


Fig. 3 Distributions of $^{239+240}\text{Pu}$ and ^{137}Cs activities in the surface soils of equal elevation paddy field in Longji Rice Terraces. **a** With an elevation of 860 m in PZTF. **b** With an elevation of 970 m in JRYTF

of $^{239+240}\text{Pu}$ and ^{137}Cs were $0.215 \pm 0.016 - 0.335 \pm 0.009$ mBq/g and $3.40 \pm 0.18 - 6.31 \pm 0.25$ mBq/g, respectively, with the mean values of 0.270 ± 0.046 mBq/g ($n=7$) and 5.27 ± 1.09 mBq/g ($n=7$). Figure 3b shows the distributions of $^{239+240}\text{Pu}$ and ^{137}Cs in the surface soils at an elevation of 970 m in the JRYTF. The activities of $^{239+240}\text{Pu}$ and ^{137}Cs were $0.214 \pm 0.017 - 0.734 \pm 0.046$ mBq/g and $3.44 \pm 0.18 - 4.92 \pm 0.22$ mBq/g, respectively, with the mean values of 0.432 ± 0.172 mBq/g and 4.18 ± 0.49 mBq/g. At the same elevation and with little variation in organic matter content, the activities of $^{239+240}\text{Pu}$ and ^{137}Cs at different sites showed discrepancies, indicating that the slope gradient was a significant factor in the discrepancy.

Similar to the staircase gradient, here, we define the angle (α) between the slope line of adjacent sampling sites and the horizontal plane as the slope gradient of the terraces

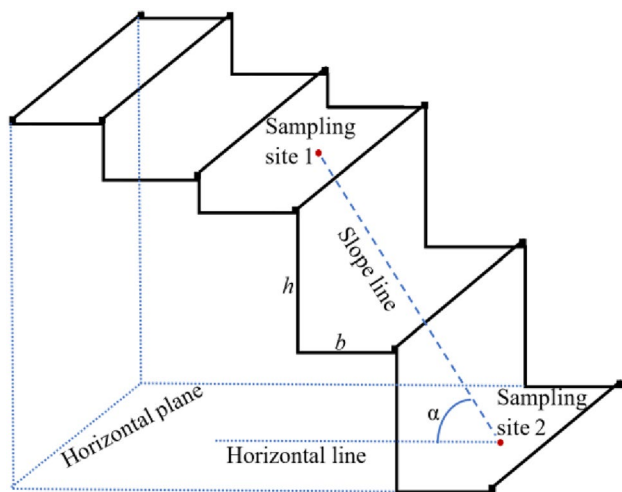


Fig. 4 Schematic diagram of the slope gradient between adjacent sampling sites of the terraces

between adjacent sampling sites (Fig. 4). The slope gradient was determined by the width (b) of the horizontal terraces at each level and the height (h) between them and the upper or lower terraces, which reflected the steepness of the terraced section. Figure 5a shows the slope gradient distribution between two adjacent sampling sites in the PZTF. The slope gradient first decreased and then increased with elevation from 900 to 790 m, which is the opposite of the distribution trends shown for the activities of $^{239+240}\text{Pu}$ and ^{137}Cs , indicating that the larger the slope gradient, the lower the activities of $^{239+240}\text{Pu}$ and ^{137}Cs and the greater the soil erosion. This is consistent with the results for sloping cultivated fields in Nanchong of Sichuan and Kaixian of Chongqing [55]. Khodadadi et al. [24] and Su et al. [25] reported that soil erosion affected the distribution of plutonium and ^{137}Cs in hillslope soils. Li et al. [53] and Van Oost et al. [54] also reported that slope gradient is the most important factor affecting the spatial variability of soil erosion rates.

The activities of $^{239+240}\text{Pu}$ and ^{137}Cs at an elevation of 930 m (P1#1_0-5) were lowest, except for that with an elevation of 790 m (P16). However, the slope gradient (9.4°) between this site P1#1_0-5 and the sampling site P11 was low (Fig. 2a and Fig. 5a). This is inconsistent with the rule that the greater the slope gradient, the lower are the activities of $^{239+240}\text{Pu}$ and ^{137}Cs . This may be due to the fact that the slope gradient between this site (P1#1_0-5, located at the top of the terrace slope closest to and directly below the observation platform) and the observation platform should be the largest. Serious soil erosion usually occurs at the top of slopes in sloping and terraced farmlands without soil material supplement [25]. This slope gradient exacerbated the scouring of the soil at this site by the rapid runoff above it (especially the concentrated rainwater from the observation platform), and there was insufficient soil replenishment at this site,

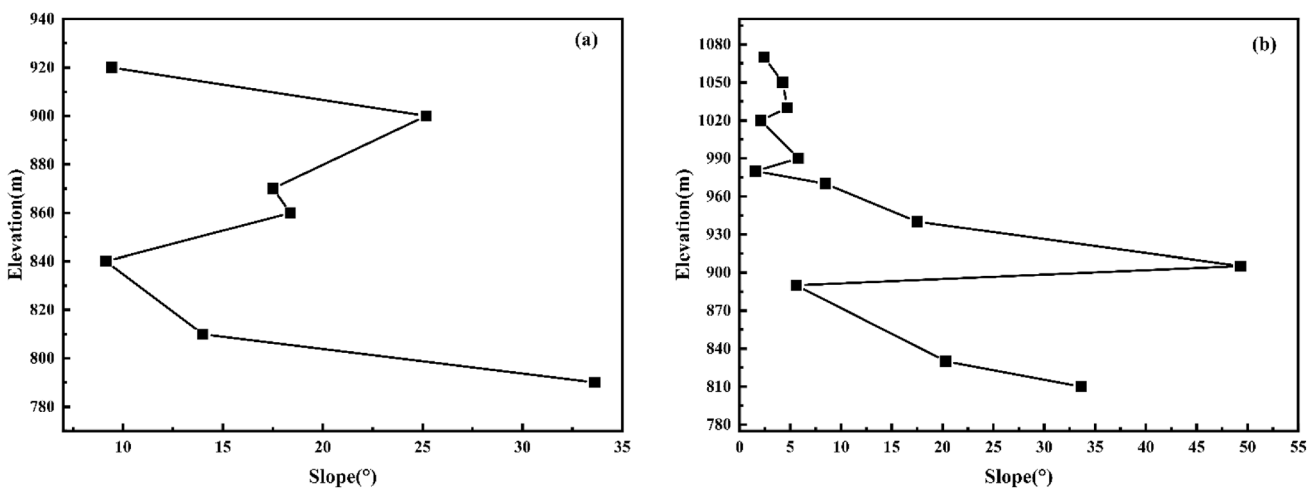


Fig. 5 Distribution of slope gradient in the adjacent surface soil sample site in Longji Rice Terraces. a PZTF. b JRYTF

resulting in the lowest activities of $^{239+240}\text{Pu}$ and ^{137}Cs . The slope gradient (9.2°) between the sample sites with elevations of 860 m (PH11) and 840 m (P14) was smaller than that (18.4°) between the samples with elevations of 860 m and 870 m (P13), whereas the maximum activity of $^{239+240}\text{Pu}$ and ^{137}Cs was not at an elevation of 840 m but at the elevations of 860 m and 870 m place. This is due to the influence of existing trails, which are paved with stones between sites at elevations of 860–840 m (Fig. 1a). The trail impeded the movement of the soil to lower elevations from an elevation of 860 m, whereas the concentrated water flowing on the trail intensified the scouring of the soil at an elevation of 840 m. This is similar to a previous report [32] that the concentrated water flow of rural roads may scour the soil and affect the distribution of ^{137}Cs and the soil erosion rate.

Figure 5b shows the slope gradient distribution between two adjacent sites in the JRYTF. The slope first decreased and then increased with elevation from 905 to 810 m, which is the opposite of the distribution trends shown for $^{239+240}\text{Pu}$ and ^{137}Cs dependence on elevation. The sampling site at an elevation of 1070 m (DA8) was close to the observation platform. Due to intense precipitation, irrigation, and other factors, surface runoff is accelerated by gravity and flows downward from the upper terraces, which greatly increases the runoff erosive power [56], resulting in lower activities of $^{239+240}\text{Pu}$ and ^{137}Cs at the sampling site (DA8). From elevations of 1070–905 m (DA2), the activities of $^{239+240}\text{Pu}$ and ^{137}Cs increased with a decrease in elevation, which may have been caused by the gradual decrease in the erosivity of the surface runoff due to the gradual increase in the soil carried by the surface runoff.

3.1.2 Vertical distributions of $^{239+240}\text{Pu}$ and ^{137}Cs activities in soil cores

The vertical distributions of $^{239+240}\text{Pu}$ and ^{137}Cs activities in the PZTF soil core (P1 #1) at an elevation of 930 m and the soil core (P1 #2) at an elevation of 860 m are shown in Fig. 6a and b, respectively. The activities of $^{239+240}\text{Pu}$ and ^{137}Cs in soil core P1#1 tended to be uniformly distributed within the upper 20 cm and declined exponentially below this depth. The distribution of ^{137}Cs activity in soil core P1#2 also tended to be uniformly distributed within the upper 20 cm, but the $^{239+240}\text{Pu}$ value fluctuated greatly within the upper 20 cm, and both declined exponentially below this depth. The difference in the distribution of Pu isotopes and ^{137}Cs activities in the upper 20 cm layers of soil core P1#2 may be due to rainwater immersion. At site P1#2, water immersion enhanced the reducibility of the soil, leading to a change in Pu (IV) to Pu (III), and the effect of oxide metals acting on Pu migration was weakened [57, 58, 59]. However, this soil environment had a very weak effect on ^{137}Cs because the reduction potential of Cs^+/Cs was lower than that of the soil environment. Therefore, the difference in the distribution of Pu isotopes and ^{137}Cs in the upper 20 cm layers of soil core P1#2 may be caused by the impact of rainwater immersion on the oxidation and reduction of Pu in the soil environment. The oxidation and reduction of Pu in soil greatly influences Pu mobility [60]. The difference in the distribution of $^{239+240}\text{Pu}$ activity in the upper 20-cm layers from soil cores P1#1 and P1#2 may be due to discrepancies in the soil environment. P1#1 had fewer rainwater soaking times because of its location at the top of the terraces, which may have been less affected by rainwater immersion. Previous studies [21, 25, 55] have also shown

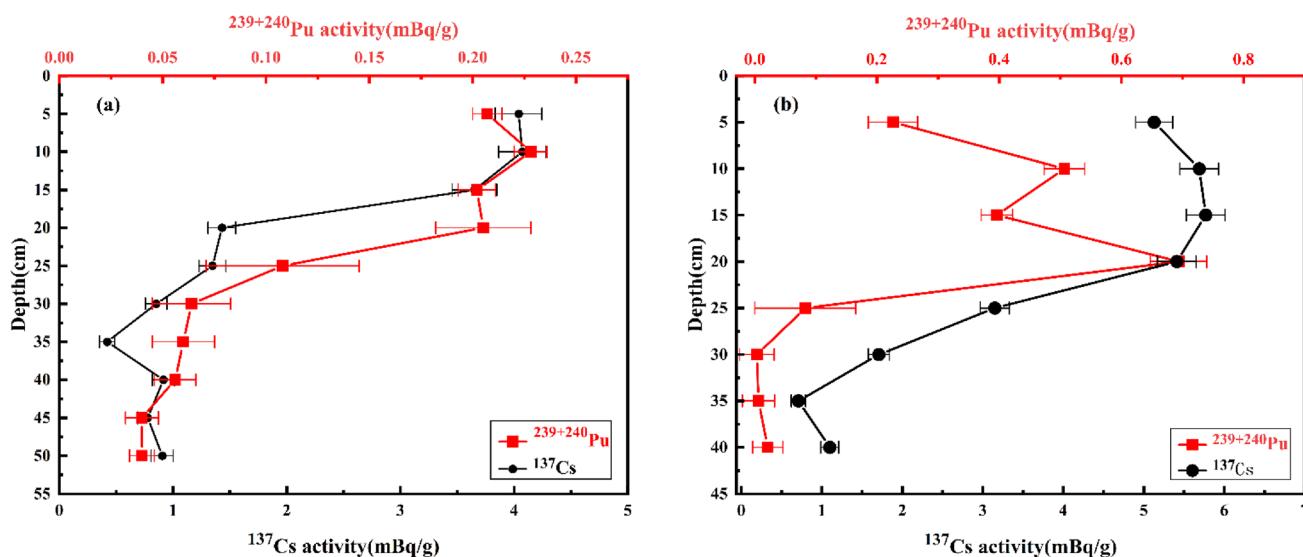


Fig. 6 (Color online) Vertical distributions of $^{239+240}\text{Pu}$ and ^{137}Cs activities in soil cores from Longji Rice Terraces. a P1#1. b P1#2

that the vertical distributions of $^{239+240}\text{Pu}$ and ^{137}Cs in the plow layer were basically uniform. Therefore, the vertical distributions of $^{239+240}\text{Pu}$ and ^{137}Cs in the two soil cores indicated that the terraced plow layer depth was approximately 20 cm, and $^{239+240}\text{Pu}$ and ^{137}Cs were mixed uniformly within the upper 20 cm by tillage. The distribution of $^{239+240}\text{Pu}$ and ^{137}Cs activities below the plow layer reflects their downward migration. The relatively high $^{239+240}\text{Pu}$ and ^{137}Cs activities within the upper 20 cm layer are also consistent with the ^{137}Cs results of the plow layer in the earth-banked terraces of the Yimeng Mountains [56].

The mean activities of $^{239+240}\text{Pu}$ and ^{137}Cs in the soil core P1#2 (0.242 ± 0.252 and 3.58 ± 2.17 mBq/g, respectively) are twice those of P1#1 (0.121 ± 0.080 and 1.84 ± 1.46 mBq/g, respectively), and the maximum activities of $^{239+240}\text{Pu}$ and ^{137}Cs (0.693 ± 0.046 and 5.77 ± 0.24 mBq/g, respectively) are also higher than that of P1#1 (0.228 ± 0.008 and 4.07 ± 0.20 mBq/g, respectively), indicating a different extent of soil erosion at two sites.

3.2 Inventories of $^{239+240}\text{Pu}$ and ^{137}Cs in soil cores

Calculated the inventories by integrating $^{239+240}\text{Pu}$ content and ^{137}Cs content in all layers from the cores P1#1 and P1#2 (Fig. 6), we calculated that the inventories of $^{239+240}\text{Pu}$ in soil cores P1#1 and P1#2 were 81.51 Bq/m^2 (surface layer accounted for 14.87%) and 119.28 Bq/m^2 (surface layer accounted for 11.10%), respectively. And the ^{137}Cs inventories in soil cores P1#1 and P1#2 were 1232.86 Bq/m^2 (surface layer accounted for 16.42%) and 1827.61 Bq/m^2 (surface layer accounted for 19.16%), respectively.

Table 2 lists the locations, elevations, precipitations, and inventories of $^{239+240}\text{Pu}$ and ^{137}Cs of Longji Rice Terraces and the previous work. The mean inventories of $^{239+240}\text{Pu}$ and ^{137}Cs in Longji Rice Terraces were 100.40 and 1530.24 Bq/m^2 , respectively. The mean inventory of $^{239+240}\text{Pu}$ was higher than the result (63 Bq/m^2) of forest soil in Guiyang of Guizhou [42] but within the range

($36 - 410 \text{ Bq/m}^2$) in the $20 - 30^\circ\text{N}$ band summarized by Cao et al. [63]. The mean inventory of ^{137}Cs was higher than that previous studies in Kaiyuan [61] and Libo [62], but within the range ($414.42 - 3140.88 \text{ Bq/m}^2$, decay-corrected to 2021) in the $20-30^\circ\text{N}$ band summarized by Tagami et al. [64]. The global inventory of plutonium deposited at a specific location may be related to precipitation, elevation, latitude, and other factors [65]. As shown in Table 2, the latitudes of Longji Rice Terraces, Guiyang, Kaiyuan, and Libo are similar, and the elevation of Longji Rice Terraces is lower than that of Guiyang but similar to that of Libo. The precipitation of Longji Rice Terraces (1900 mm/y) was higher than that of Guiyang (1130 mm/y) and Libo (1470 mm/y), and the high plutonium inventory and ^{137}Cs inventory of Longji Rice Terraces may be due to the relatively high precipitation.

3.3 Soil erosion rate

The soil erosion rate of cultivated land can be estimated by a simplified mass balance model [4, 66, 67]:

$$I_m = I_f \left(1 - \frac{h}{H}\right)^{N-1963}, \quad (1)$$

where I_m is the measured inventory of $^{239+240}\text{Pu}$ or ^{137}Cs in the eroded soil core (Bq/m^2), I_f is the background value of $^{239+240}\text{Pu}$ or ^{137}Cs inventory (Bq/m^2) in the study area, H is the depth of the plow layer (cm), h is the erosion thickness (cm/a), and N is the sampling year. Thus, the soil erosion rate E ($\text{t/ha}\cdot\text{a}$) is given by the expression [4]:

$$E = 100 \cdot h \cdot B, \quad (2)$$

where B is the soil bulk density (g/cm^3).

A background inventory (I_f) of $^{239+240}\text{Pu}$ or ^{137}Cs in the study area is crucial for estimating soil erosion. The traditional approach is to take an inventory of an undisturbed and flat reference site, which represents the background

Table 2 Locations, elevations, precipitations, and inventories of $^{239+240}\text{Pu}$ and ^{137}Cs of Longji Rice Terraces (LJRT) and previous work

Sample site	Location	Elevation (m)	Precipitation (mm/y)	$^{239+240}\text{Pu}$ inventory (Bq/m^2)	^{137}Cs inventory (Bq/m^2)	References
Guiyang	$106^\circ 40' 10''\text{E}$, $26^\circ 39' 23''\text{N}$	1349	1130	63	–	[42]
Kaiyuan	$103^\circ 26' 48.37''\text{E}$, $23^\circ 29' 20.15''\text{N}$	–	904	–	859.29	[61]
Libo	$107^\circ 37'\text{E} - 108^\circ 18'\text{E}$, $25^\circ 7'\text{N} - 25^\circ 9'\text{N}$	860–1020	1470	–	723.29	[62]
LJRT	$110^\circ 7'\text{E}$, $25^\circ 45'\text{N}$	860–930	1900	100.40	1530.24	This study

The ^{137}Cs inventories were decay-corrected to 2021

inventory of the study area. However, this approach is not applicable to the Longji Rice Terraces. If site P1#1 is taken as a reference site, we will obtain the unreasonable result that there is only soil deposition in the terraces, except for the top site P1#1 and the bottom site, because the lowest activity concentrations of $^{239+240}\text{Pu}$ and ^{137}Cs on the surface (Fig. 2a) appeared at 930 m (the top site P1#1) and 790 m (the bottom site). It is also inappropriate to use site P1#2 as a reference because it is impossible to determine whether the soil flowing into and out of site P1 #2 is in equilibrium. In addition, the inventories of $^{239+240}\text{Pu}$ and ^{137}Cs were higher than those of nearby areas (Table 2) because of the relatively high precipitation in the study area; therefore, neither of the sites listed in Table 2 is an ideal reference site. It is also difficult to find an ideal undisturbed and flat reference site in the study area because of its unique erosional environment (special topography and geomorphological characteristics). Moreover, when the surface soil was eroded, the depth of the plow layer was approximately constant owing to the same tillage method; therefore, the deeper soil under the original plow layer was turned over and mixed evenly with the upper soil, which diluted the $^{239+240}\text{Pu}$ and ^{137}Cs in the soil of the original plow layer, resulting in the redistribution of $^{239+240}\text{Pu}$ and ^{137}Cs in the surface soil from the terraces. Therefore, the distributions of $^{239+240}\text{Pu}$ and ^{137}Cs in the surface soils from the studied area of Longji Rice Terraces can reflect soil erosion, and the mean surface activities of $^{239+240}\text{Pu}$ and ^{137}Cs can be used as the background values of surface activity in the studied area. Therefore, we estimated the background values of $^{239+240}\text{Pu}$ and ^{137}Cs inventories from the mean activities of $^{239+240}\text{Pu}$ and ^{137}Cs , respectively, in surface soil.

The $^{239+240}\text{Pu}$ in the surface layers (0–5 cm) of soil cores P1#1 and P1#2 accounted for 14.87% and 11.10%, respectively, of the total soil core inventory, with a mean value of 12.98%. The ^{137}Cs in the surface layers of soil cores P1#1 and P1#2 accounted for 19.15% and 16.42% of the total soil core inventory, respectively, with a mean value of 17.79%. The inventories of $^{239+240}\text{Pu}$ and ^{137}Cs in the surface layer were 14.67 and 303.92 Bq/m², respectively,

which were derived from the mean activity of $^{239+240}\text{Pu}$ (0.253 mBq/g) and ^{137}Cs (5.24 mBq/g) as well as the bulk density (1.16 g/cm³) in the surface samples from PZTF. Then the background values of 113.05 Bq/m² for $^{239+240}\text{Pu}$ and 1708.38 Bq/m² for ^{137}Cs were estimated by the proportion (12.98% for $^{239+240}\text{Pu}$ and 17.79% for ^{137}Cs , respectively) of inventory in the surface layer. The background values obtained using this method were slightly different from the mean inventories of $^{239+240}\text{Pu}$ and ^{137}Cs from cores P1 #1 and P1 #2 in the study area. For $^{239+240}\text{Pu}$, the calculated background value was 113.05 Bq/m² and the mean inventory from P1#1 and P1#2 cores was 100.4 Bq/m², and the difference between them was only 11.6%. For ^{137}Cs , the difference between the calculated background value of 1708.38 Bq/m² and the mean inventory of 1530.24 Bq/m² was only 12.5%. Therefore, the background values of the study area estimated using our method are reasonable and credible.

Soil erosion rates were calculated using $^{239+240}\text{Pu}$ and ^{137}Cs methods (Table 3). The result showed that the erosion rates calculated by the $^{239+240}\text{Pu}$ method were 13.04 t/(ha·a) for P1#1 site and -2.15 t/(ha·a) for the P1#2 site, which is consistent with the values of 13.01 t/(ha·a) and -2.70 t/(ha·a) by ^{137}Cs method. The erosion rates were negative, indicating net soil deposition at site P1 #2.

P1#1 was near the observation platform, and the slope gradient between it and the observation platform was steeper, resulting in severe erosion at P1#1 and no soil replenishment at that location. Sampling site P1#2 was located on the contour at an elevation of 860 m (near PH11). The slope gradient was approximately 18.4°, which was gentler than the slope gradient between the upper terraces at higher elevations. Therefore, the eroded soil from the upper terraces was easily deposited in P1#2. Soil erosion rates at sampling site P1#1 were much higher than those at P1#2, again confirming that local landform features (e.g., slope gradient variation) are the main factors influencing soil erosion in the Longji Rice Terraces.

The mean erosion rates (i.e., the arithmetic mean of the erosion rates at sampling points P1#1 and P1#2) of Longji Rice Terraces estimated by the $^{239+240}\text{Pu}$ method

Table 3 Soil erosion rates estimated by $^{239+240}\text{Pu}$ and ^{137}Cs methods

Sampling sites	Erosion rates (t·ha ⁻¹ ·a ⁻¹)		References
	$^{239+240}\text{Pu}$ method	^{137}Cs method	
P1#1	13.04	13.01	This study
P1#2	-2.15	-2.70	This study
Terraces in the Yimeng Mountains	-	27	[56]
Terraces in Zhongxian County, Chongqing	-	56.47 ^a	[26]
Dapotou depression, Yunnan	-	6.32	[61]
Cultivated land of Pingguo in Guangxi	-	19.4 ^a	[68]
Cultivated land of Huanjiang in Guangxi	-	0.22	[69]

^aMean value

(5.44 t/(ha·a)) and the ^{137}Cs method (5.16 t/(ha·a)) are basically consistent with that of the Dapotou depression in Yunnan Province (6.32 t/(ha·a)) [61], but higher than that of the cultivated land in Huanjiang County, Guangxi (0.22 t/(ha·a)) [69]. The Dapotou depression area (23° 36′48.04″–23° 37′28.10″ N) and the Longji Rice Terraces are both hillside cultivated lands with similar latitudes; this is a possible reason why the mean erosion rates of both are similar. Higher precipitation (1900 mm/y for Longji Rice Terraces and 1390 mm/y for Huanjiang County) may lead to higher soil erosion in the Longji Rice Terraces than in Huanjiang County. In addition, the reported cultivated land in Huanjiang County has been partially reclaimed, and some of the cultivated land was converted from cultivated land to grassland in 2004. The diverse land-use types and high vegetation cover may be other reasons for the lower soil erosion rate in Huanjiang County. This may be due to the higher vegetation cover of grasslands compared to cultivated land, and the interlaced plant roots in grasslands can inhibit soil erosion [36]. Moreover, the mean soil erosion rate of Longji Rice Terraces is much lower of the steep sloping terraces (56.47 t/(ha·a)) in Zhongxian County of Chongqing [26], the earth-banked terraces (27 t/(ha·a)) in the Yimeng Mountains [56], and the cultivated land (19.4 t/(ha·a)) in Pingguo City of Guangxi [68]. The soil of the steep-slope terraces in Zhongxian County is purple with loose parent rock that easily disintegrates and has faster soil loss. The Longji Rice Terraces are known as a hundred-stage terrace system, whereas the Yimeng Mountain terrace study area is only a seven-stage terrace system, which may have led to a lower erosion rate of the Longji Rice Terraces. This may be because the terraces changed the slope gradient of the original hillslope, flattening the terraced plots at all levels. The more steps there were, the shorter the slope length of each terrace, and the terrace fields could slow or prevent rapid surface runoff due to the interception of runoff water and a shorter slope length, which significantly reduced runoff and soil erosion rates [70]. In addition, Longji Rice Terraces are cultivated once a year, while in Yimeng Mountain, they are cultivated twice a year (wheat-corn rotation), and lower tillage frequency may be another reason for the lower erosion rate in Longji Rice Terraces. It has been reported that there is a sinkhole in the cultivated land in Pingguo City, and obvious underground erosion is a possible reason why the soil erosion rate in this area is higher than that of the Longji Rice Terraces.

In summary, the results show that the differences in soil erosion rates in the above-mentioned areas are mainly related to precipitation, landform features, soil structure and properties, vegetation coverage, crop type, and tillage frequency.

4 Conclusion

The activities of $^{239+240}\text{Pu}$ and ^{137}Cs in the surface soil were 0.089–0.734 mBq/g ($n=33$) and 1.80–7.88 mBq/g ($n=33$), respectively. All $^{240}\text{Pu}/^{239}\text{Pu}$ atom ratios were in good agreement with the global fallout value, indicating that plutonium in Longji Rice Terrace soils originates from the global fallout. The inventories of $^{239+240}\text{Pu}$ and ^{137}Cs were 81.51–119.28 Bq/m² and 1232.86–1827.61 Bq/m², respectively. The erosion rates calculated using the $^{239+240}\text{Pu}$ method and ^{137}Cs methods were consistent. The distributions of $^{239+240}\text{Pu}$ and ^{137}Cs and the soil erosion rates at the different sample sites were mainly caused by local landform features, especially the slope gradient. The erosion rate of the P1#1 site calculated by the $^{239+240}\text{Pu}$ method (13.04 t/(ha·a)) and the ^{137}Cs method (13.01 t/(ha·a)) showed that there was severe soil erosion and necessary measurements should be taken to reduce it. Plutonium, as a potential tracer, can replace ^{137}Cs in the future and plays an important role in soil erosion research.

Author contributions All authors contributed to the study conception and design. Material preparation, data collection, and analysis were performed by Yong-Jing Guan, Wu Chen, Shen-Zhen Wang, Yu-Xin Hua, Qiao-Yan Jing, Zhi-Yong Liu, Chun-Ping Huang, De-Yu Wang, Hui-Juan Wang, Xian-Wen He, Mario De Cesare, Liang-Jia Cui, Hua He, Kai-Di Fan, and Zi-Chen Guo. The first draft of the manuscript was written by Yong-Jing Guan and Wu Chen, and all authors commented on previous versions of the manuscript. All authors read and approved the final manuscript.

Data Availability The data that support the findings of this study are openly available in Science Data Bank at <https://doi.org/10.57760/sciencedb.j00186.00060> and <https://cstr.cn/31253.11.sciencedb.j00186.00060>.

Open Access This article is licensed under a Creative Commons Attribution 4.0 International License, which permits use, sharing, adaptation, distribution and reproduction in any medium or format, as long as you give appropriate credit to the original author(s) and the source, provide a link to the Creative Commons licence, and indicate if changes were made. The images or other third party material in this article are included in the article's Creative Commons licence, unless indicated otherwise in a credit line to the material. If material is not included in the article's Creative Commons licence and your intended use is not permitted by statutory regulation or exceeds the permitted use, you will need to obtain permission directly from the copyright holder. To view a copy of this licence, visit <http://creativecommons.org/licenses/by/4.0/>.

References

1. L. Mabit, F. Zapata, G. Dercon et al., Assessment of soil erosion and sedimentation: the role of fallout radionuclides. IAEA, 3–26 (2014). <https://www.osti.gov/etdweb/biblio/22311433>
2. F. Zapata, *Handbook for the assessment of soil erosion and sedimentation using environmental radionuclides* (Springer, Dordrecht, 2002)

3. L. Mabit, K. Meusburger, E. Fulajtar et al., The usefulness of ^{137}Cs as a tracer for soil erosion assessment: A critical reply to Parsons and Foster (2011). *Earth Sci. Rev.* **127**, 300–307 (2013). <https://doi.org/10.1016/j.earscirev.2013.05.008>
4. Y.H. Xu, J.X. Qiao, S.M. Pan et al., Plutonium as a tracer for soil erosion assessment in northeast China. *Sci. Total Environ.* **511**, 176–185 (2015). <https://doi.org/10.1016/j.scitotenv.2014.12.006>
5. C. Wulandari, A. Waris, S. Permana et al., Evaluating the JEFF 3.1, ENDF/B-VII. 0, JENDL 3.3, and JENDL 4.0 nuclear data libraries for a small 100 MWe molten salt reactor with plutonium fuel. *Nucl. Sci. Tech.* **33**(12), 165 (2022). <https://doi.org/10.1007/s41365-022-01141-8>
6. Z.X. Fang, M. Yu, Y.G. Huang et al., Theoretical analysis of long-lived radioactive waste in pressurized water reactor. *Nucl. Sci. Tech.* **32**(7), 72 (2021). <https://doi.org/10.1007/s41365-021-00911-0>
7. E. Sholkovitz, The geochemistry of plutonium in fresh and marine water environments. *Earth Sci. Rev.* **19**(2), 95–161 (1983). [https://doi.org/10.1016/0012-8252\(83\)90029-6](https://doi.org/10.1016/0012-8252(83)90029-6)
8. M. Dai, K.O. Buesseler, S.M. Pike, Plutonium in groundwater at the 100K-Area of the US DOE Hanford Site. *J. Contam. Hydrol.* **76**(3–4), 167–189 (2005). <https://doi.org/10.1016/j.jconhyd.2004.08.004>
9. J. Zheng, K. Tagami, Y. Watanabe et al., Isotopic evidence of plutonium release into the environment from the Fukushima DNPP accident. *Sci. Rep.* **2**, 304 (2012). <https://doi.org/10.1038/srep00304>
10. J.X. Qiao, X.L. Hou, M. Miro et al., Determination of plutonium isotopes in waters and environmental solids: A review. *Anal. Chim. Acta.* **652**(1–2), 66–84 (2009). <https://doi.org/10.1016/j.aca.2009.03.010>
11. T. Warneke, I.W. Croudace, P.E. Warwick et al., A new ground-level fallout record of uranium and plutonium isotopes for northern temperate latitudes. *Earth Planet. Sci. Lett.* **203**(3–4), 1047–1057 (2002). [https://doi.org/10.1016/S0012-821x\(02\)00930-5](https://doi.org/10.1016/S0012-821x(02)00930-5)
12. Y.J. Guan, H.J. Wang, M. De Cesare et al., The AMS measurement of ^{236}U at CIRCE. *Nucl. Sci. Tech.* **28**(7), 98 (2017). <https://doi.org/10.1007/s41365-017-0252-5>
13. M. De Cesare, L. Gialanella, D. Rogalla et al., Actinides AMS at CIRCE in Caserta (Italy). *Nucl. Instrum. Meth. Phys. Res. Sect. B* **268**(7–8), 779–783 (2010). <https://doi.org/10.1016/j.nimb.2009.10.029>
14. S.M. Qin, X.G. Wang, X.X. Lan et al., A primary study on biological behavior of aluminum using ^{26}Al -AMS. *Nucl. Sci. Tech.* **27**(3), 53 (2016). <https://doi.org/10.1007/s41365-016-0065-y>
15. S. Çam Kaynar, Annual effective dose values from ^{137}Cs activity concentrations in soils of Manisa, Turkey. *Nucl. Sci. Tech.* **29**, 100 (2018). <https://doi.org/10.1007/s41365-018-0440-y>
16. A.S. Alaamer, Characterization of ^{137}Cs in Riyadh Saudi Arabia Soil Samples. *World Journal of Nuclear Science and Technology* **2**(4), 161–164 (2012). <https://doi.org/10.4236/wjnst.2012.24024>
17. A. Jabbar, K. Khan, T. Jabbar et al., Radioactive contents and background doses from northern alluvial sediment plains between rivers Ravi and Chenab Pakistan. *Nucl. Sci. Tech.* **27**(4), 94 (2016). <https://doi.org/10.1007/s41365-016-0085-7>
18. J. Wu, Y. Wang, W. Sun et al., Atmospheric radionuclides from Fukushima Dai-ichi nuclear accident detected in Lanzhou China. *Nucl. Sci. Tech.* **26**(4), 117–122 (2015). <https://doi.org/10.13538/j.1001-8042/nst.26.040604>
19. H.T. Jia, S.T. Lin, S.K. Liu et al., High-accuracy measurement of Compton scattering in germanium for dark matter searches. *Nucl. Sci. Tech.* **33**(12), 157 (2022). <https://doi.org/10.1007/s41365-022-01148-1>
20. Y.Y. Zheng, Z.H. Zhang, Q. Li et al., Design of an energetic particle radiation diagnostic spectroscopy system based on national core chips and Qt on Linux in EAST. *Nucl. Sci. Tech.* **32**(7), 68 (2021). <https://doi.org/10.1007/s41365-021-00906-x>
21. Y.H. Xu, J.X. Qiao, X.L. Hou et al., Plutonium in soils from north-east China and its potential application for evaluation of soil erosion. *Sci. Rep.* **3**(1), 3506 (2013). <https://doi.org/10.1038/srep03506>
22. C. Alewell, A. Pitois, K. Meusburger et al., $^{239+240}\text{Pu}$ from “contaminant” to soil erosion tracer: Where do we stand? *Earth Sci. Rev.* **172**, 107–123 (2017). <https://doi.org/10.1016/j.earscirev.2017.07.009>
23. T. Yu, J. Yang, Z.Y. Wang, Adsorption behaviour of Eu(III) on natural bamboo fibres: effects of pH, humic acid, contact time, and temperature. *Nucl. Sci. Tech.* **31**(1), 4 (2020). <https://doi.org/10.1007/s41365-019-0710-3>
24. M. Khodadadi, C. Alewell, M. Mirzaei et al., Deforestation effects on soil erosion rates and soil physicochemical properties in Iran: a case study of using fallout radionuclides in a Chernobyl contaminated area. *SOIL Discussions*, 1–41 (2021). <https://doi.org/10.5194/soil-2021-2>
25. Z.A. Su, L.J. Wang, Y.H. Liu et al., ^{137}Cs tracing of the spatial patterns in soil redistribution, organic carbon and total nitrogen in the southeastern Tibetan Plateau. *Int. Soil Water Conserv. Res.* **11**(1), 86–96 (2022). <https://doi.org/10.1016/j.iswcr.2022.05.001>
26. Z. A. Su, J. H. Zhang, Effects of tillage erosion on soil redistribution in a purple soil with steep sloping terraces. 2010 International Conference on Management and Service Science, 1–4 (2010). <https://doi.org/10.1109/ICMSS.2010.5577125>
27. C. Alewell, K. Meusburger, G. Juretzko et al., Suitability of $^{239+240}\text{Pu}$ and ^{137}Cs as tracers for soil erosion assessment in mountain grasslands. *Chemosphere* **103**, 274–280 (2014). <https://doi.org/10.1016/j.chemosphere.2013.12.016>
28. K.X. Zhang, S.M. Pan, Y.H. Xu et al., Using $^{239+240}\text{Pu}$ atmospheric deposition and a simplified mass-balance model to re-estimate the soil erosion rate: a case study of Liaodong Bay in China. *J. Radioanal. Nucl. Chem.* **307**(1), 599–604 (2015). <https://doi.org/10.1007/s10967-015-4208-0>
29. N. Yamagata, S. Matsuda, K. Kodaira, Run-off of caesium-137 and strontium-90 from rivers. *Nature* **200**, 668–669 (1963). <https://doi.org/10.1038/200668b0>
30. J.C. Ritchie, J.R. Mchenry, Application of radioactive fallout Cesium-137 for measuring soil erosion and sediment accumulation rates and patterns: A review. *J. Environ. Qual.* **19**(2), 215–233 (1990). <https://doi.org/10.2134/jeq1990.00472425001900020006x>
31. P. Porto, D.E. Walling, A. Capra, Using ^{137}Cs and $^{210}\text{Pb}_{\text{ex}}$ measurements and conventional surveys to investigate the relative contributions of interrill/rill and gully erosion to soil loss from a small cultivated catchment in Sicily. *Soil Tillage Res.* **135**, 18–27 (2014). <https://doi.org/10.1016/j.still.2013.08.013>
32. Z.A. Su, D.H. Xiong, W. Deng et al., ^{137}Cs tracing dynamics of soil erosion, organic carbon, and total nitrogen in terraced fields and forestland in the Middle Mountains of Nepal. *J. Mount. Sci.* **13**(10), 1829–1839 (2016). <https://doi.org/10.1007/s11629-015-3581-z>
33. W. Schimmack, K. Auerswald, K. Bunzl, Can $^{239+240}\text{Pu}$ replace ^{137}Cs as an erosion tracer in agricultural landscapes contaminated with Chernobyl fallout? *J. Environ. Radioact.* **53**(1), 41–57 (2001). [https://doi.org/10.1016/S0265-931X\(00\)00117-X](https://doi.org/10.1016/S0265-931X(00)00117-X)
34. W. Schimmack, K. Auerswald, K. Bunzl, Estimation of soil erosion and deposition rates at an agricultural site in Bavaria, Germany, as derived from fallout radiocesium and plutonium as tracers. *Naturwissenschaften* **89**(1), 43–46 (2002). <https://doi.org/10.1007/s00114-001-0281-z>

35. W.T. Hoo, L.K. Fifield, S.G. Tims et al., Using fallout plutonium as a probe for erosion assessment. *J. Environ. Radioact.* **102**(10), 937–942 (2011). <https://doi.org/10.1016/j.jenvrad.2010.06.010>
36. Y. Liu, X. Hou, J. Qiao et al., Evaluation of soil erosion rates in the hilly-gully region of the Loess Plateau in China in the past 60 years using global fallout plutonium. *CATENA* **220**, 106666 (2023). <https://doi.org/10.1016/j.catena.2022.106666>
37. Y. Guan, J. Mai, H. Wang et al., Plutonium isotopes and radionuclides in corals around Weizhou land in Beibu Gulf, China. *Appl. Radiat. Isot.* **176**, 109873 (2021). <https://doi.org/10.1016/j.apradiso.2021.109873>
38. Y. Guan, S. Sun, S. Sun et al., Distribution and sources of plutonium along the coast of Guangxi, China. *Nucl. Instrum. Meth. Phys. Res. Sect. B* **437**, 61–65 (2018). <https://doi.org/10.1016/j.nimb.2018.09.047>
39. Y. Guan, P. Zhang, C. Huang et al., Vertical distribution of Pu in forest soil in Qinghai-Tibet Plateau. *J. Environ. Radioact.* **229**, 106548 (2021). <https://doi.org/10.1016/j.jenvrad.2021.106548>
40. J.M. Kelley, L.A. Bond, T.M. Beasley, Global distribution of Pu isotopes and ^{237}Np . *Sci. Total Environ.* **237–238**, 483–500 (1999). [https://doi.org/10.1016/s0048-9697\(99\)00160-6](https://doi.org/10.1016/s0048-9697(99)00160-6)
41. R.R. Wang, J.Y. Mai, Y.J. Guan et al., Radionuclides in the environment around the uranium mines in Guangxi China. *Appl. Radiat. Isot.* **159**, 109098 (2020). <https://doi.org/10.1016/j.apradiso.2020.109098>
42. W.T. Bu, J. Zheng, Q.J. Guo et al., Vertical distribution and migration of global fallout Pu in forest soils in southwestern China. *J. Environ. Radioact.* **136**, 174–180 (2014). <https://doi.org/10.1016/j.jenvrad.2014.06.010>
43. H. Wang, Y. Ni, W. Men, Z. Wang, M. Liu, D. Xiao, J. Zheng, Distributions of fallout ^{137}Cs , $^{239+240}\text{Pu}$ and ^{241}Am in a soil core from South Central China. *J. Environ. Radioact.* **251**, 106971 (2022). <https://doi.org/10.1016/j.jenvrad.2022.106971>
44. H.Q. Liao, J. Zheng, F.C. Wu et al., Determination of plutonium isotopes in freshwater lake sediments by sector-field ICP-MS after separation using ion-exchange chromatography. *Appl. Radiat. Isot.* **66**(8), 1138–1145 (2008). <https://doi.org/10.1016/j.apradiso.2008.01.001>
45. Z.Y. Liu, J. Zheng, S.M. Pan et al., Anthropogenic plutonium in the North Jiangsu tidal flats of the Yellow Sea in China. *Environ. Monit. Assess.* **185**(8), 6539–6551 (2013). <https://doi.org/10.1007/s10661-012-3045-7>
46. Y.Y. Ni, Z.T. Wang, Q.J. Guo et al., Distinctive distributions and migrations of $^{239+240}\text{Pu}$ and ^{241}Am in Chinese forest, grassland and desert soils. *Chemosphere* **212**, 1002–1009 (2018). <https://doi.org/10.1016/j.chemosphere.2018.09.021>
47. P. Lindahl, P. Worsfold, M. Keith-Roach et al., Temporal record of Pu isotopes in inter-tidal sediments from the northeastern Irish Sea. *Sci. Total Environ.* **409**(23), 5020–5025 (2011). <https://doi.org/10.1016/j.scitotenv.2011.08.019>
48. M. Yamamoto, K. Komura, M. Sakanoue, Discrimination of the plutonium due to atomic explosion in 1945 from global fallout plutonium in Nagasaki soil. *J. Radiat. Res.* **24**(3), 250–258 (1983). <https://doi.org/10.1269/jrr.24.250>
49. Y. Muramatsu, W. Rühm, S. Yoshida et al., Concentrations of ^{239}Pu and ^{240}Pu and their isotopic ratios determined by ICP-MS in soils collected from the Chernobyl 30-km zone. *Environ. Sci. Technol.* **34**(14), 2913–2917 (2000). <https://doi.org/10.1021/es0008968>
50. Q.J. Guo, Y.Y. Ni, S.X. Li, Distribution of important transuranium nuclides in Chinese environmental soil. *Atomic Energy Science and Technology* **53**(10), 2083 (2019). <https://doi.org/10.7538/yzk.2019.53.10.2083> (in Chinese)
51. Q. Cheng, S. Wang, T. Peng, L. Cao, X. Zhang, S.J. Buckerfield, A.L. Collins, Sediment sources, soil loss rates and sediment yields in a Karst plateau catchment in Southwest China. *Agric. Ecosys. Environ.* **304**, 107114 (2020). <https://doi.org/10.1016/j.agee.2020.107114>
52. K. Bunzl, W. Kracke, W. Schimmack et al., Migration of fallout $^{239+240}\text{Pu}$, ^{241}Am and ^{137}Cs in the various horizons of a forest soil under pine. *J. Environ. Radioact.* **28**(1), 17–34 (1995). [https://doi.org/10.1016/0265-931X\(94\)00066-6](https://doi.org/10.1016/0265-931X(94)00066-6)
53. S. Li, D.A. Lobb, M.J. Lindstrom et al., Tillage and water erosion on different landscapes in the northern North American Great Plains evaluated using ^{137}Cs technique and soil erosion models. *CATENA* **70**(3), 493–505 (2007). <https://doi.org/10.1016/j.catena.2006.12.003>
54. K. Van Oost, W. Van Muysen, G. Govers et al., From water to tillage erosion dominated landform evolution. *Geomorphology* **72**(1–4), 193–203 (2005). <https://doi.org/10.1016/j.geomorph.2005.05.010>
55. X.B. Zhang, Y.Y. Zhang, A.B. Wen et al., Assessment of soil losses on cultivated land by using the ^{137}Cs technique in the Upper Yangtze River Basin of China. *Soil Tillage Res.* **69**(1–2), 99–106 (2003). [https://doi.org/10.1016/S0167-1987\(02\)00131-9](https://doi.org/10.1016/S0167-1987(02)00131-9)
56. Y.Q. Zhang, Y. Long, J. An et al., Spatial patterns of ^{137}Cs inventories and soil erosion from earth-banked terraces in the Yimeng Mountains China. *J. Environ. Radioact.* **136**, 1–9 (2014). <https://doi.org/10.1016/j.jenvrad.2014.04.017>
57. J.X. Qiao, X.L. Hou, Fractionation of plutonium in environmental and bio-shielding concrete samples using dynamic sequential extraction. *J. Environ. Radioact.* **101**(3), 244–249 (2010). <https://doi.org/10.1016/j.jenvrad.2009.11.007>
58. P. Lin, C. Xu, D.I. Kaplan et al., Nagasaki sediments reveal that long-term fate of plutonium is controlled by select organic matter moieties. *Sci. Total Environ.* **678**, 409–418 (2019). <https://doi.org/10.1016/j.scitotenv.2019.04.375>
59. J.A. Lucey, A. Gouzy, D. Boust et al., Geochemical fractionation of plutonium in anoxic Irish Sea sediments using an optimised sequential extraction protocol. *Appl. Radiat. Isot.* **60**(2–4), 379–385 (2004). <https://doi.org/10.1016/j.apradiso.2003.11.045>
60. D.I. Kaplan, D.I. Demirkanli, L. Gumapas et al., Eleven-year field study of Pu migration from Pu III, IV, and VI sources. *Environ. Sci. Technol.* **40**(2), 443–448 (2006). <https://doi.org/10.1021/es050073o>
61. Y.Q. Li, Z.C. Jiang, Y. Yu et al., Evaluation of soil erosion and sediment deposition rates by the ^{137}Cs fingerprinting technique at different hillslope positions on a catchment. *Environ. Monit. Assess.* **192**(11), 717 (2020). <https://doi.org/10.1007/s10661-020-08680-w>
62. X.Y. Bai, X.B. Zhang, H. Chen et al., Using Cs-137 fingerprinting technique to estimate sediment deposition and erosion rates from Yongkang depression in the Karst Region of Southwest China. *Land Degrad. Dev.* **21**(5), 474–479 (2010). <https://doi.org/10.1002/ldr.983>
63. L.G. Cao, Z.C. Zhou, N. Wang et al., Quantitative assessment of the spatial distribution of $^{239+240}\text{Pu}$ inventory derived from global fallout in soils from Asia and Europe. *J. Geog. Sci.* **32**(4), 605–616 (2022). <https://doi.org/10.1007/s11442-022-1963-z>
64. K. Tagami, H. Tsukada, S. Uchida, Quantifying spatial distribution of ^{137}Cs in reference site soil in Asia. *CATENA* **180**, 341–345 (2019). <https://doi.org/10.1016/j.catena.2019.05.009>
65. S.E. Palsson, B.J. Howard, T.D. Bergan et al., A simple model to estimate deposition based on a statistical reassessment of global fallout data. *J. Environ. Radioact.* **121**, 75–86 (2013). <https://doi.org/10.1016/j.jenvrad.2012.03.006>
66. X.B. Zhang, D.E. Walling, Q. He, Simplified mass balance models for assessing soil erosion rates on cultivated land using caesium-137 measurements. *Hydrol. Sci. J.* **44**(1), 33–45 (1999). <https://doi.org/10.1080/02626669909492201>
67. R. Lal, S.G. Tims, L.K. Fifield et al., Applicability of ^{239}Pu as a tracer for soil erosion in the wet-dry tropics of northern Australia.

- Nucl. Instrum. Meth. Phys. Res. Sect. B **294**, 577–583 (2013). <https://doi.org/10.1016/j.nimb.2012.07.041>
68. W.Q. Luo, Z.C. Jiang, Q.Y. Yang et al., The features of soil erosion and soil leakage in karst peak-cluster areas of Southwest China. *J. Groundw. Sci. Eng.* **6**(1), 18–30 (2018). <https://doi.org/10.19637/j.cnki.2305-7068.2018.01.003>
69. T. Feng, H.S. Chen, V.O. Polyakov et al., Soil erosion rates in two karst peak-cluster depression basins of northwest Guangxi, China: Comparison of the RUSLE model with ^{137}Cs measurements. *Geomorphology* **253**, 217–224 (2016). <https://doi.org/10.1016/j.geomorph.2015.10.013>
70. Q.W. Zhang, Y. Li, Effectiveness assessment of soil conservation measures in reducing soil erosion in Baiquan County of Northeastern China by using ^{137}Cs techniques. *Environ. Sci. Process. Impacts* **16**(6), 1480–1488 (2014). <https://doi.org/10.1039/c3em00521f>